HIGHLIGHTS

- Difluorodithieno[3,2-*a*:2',3'-*c*]phenazine (DTPz) is applied as acceptor in TADF materials
- The time-resolved photophysical properties are studied
- Quantum-chemical analysis is used to estimate the charge-transfer character
- Different emission mechanisms are found (TADF vs RTP)
- Room temperature phosphorescence occurs from a local DTPz state

Graphical Abstract

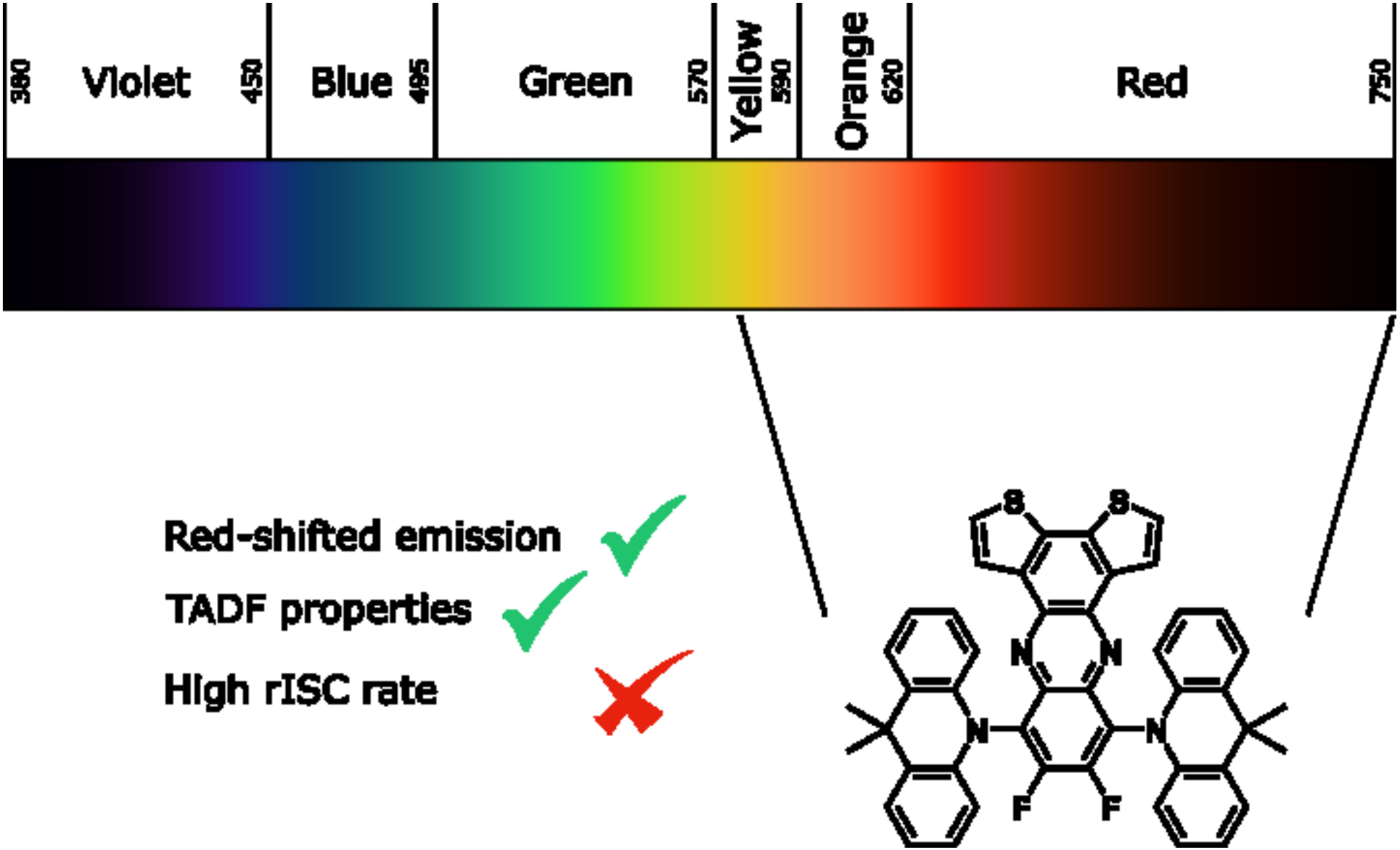

Difluorodithieno[3,2-*a*:2',3'-*c*]phenazine as a strong acceptor for materials displaying thermally activated delayed fluorescence or room temperature phosphorescence

Tom Cardeynaels,[a,b] Simon Paredis,[a] Andrew Danos,[c] Alastair Harrison,[c] Jasper Deckers,[a] Sonny Brebels,[a] Laurence Lutsen,[a] Dirk Vanderzande,[a] Andrew P. Monkman,[c] Benoît Champagne[b] and Wouter Maes[a,*]

[a] Hasselt University, Institute for Materials Research (IMO-IMOMEC), Design & Synthesis of Organic Semiconductors (DSOS), Agoralaan 1, 3590 Diepenbeek, Belgium and IMOMEC Division, IMEC, Wetenschapspark 1, 3590 Diepenbeek, Belgium
[b] University of Namur, Laboratory of Theoretical Chemistry, Theoretical and Structural Physical Chemistry Unit, Namur Institute of Structured Matter, Rue de Bruxelles 61, 5000 Namur, Belgium
[c] OEM group, Department of Physics, Durham University, South Road, Durham DH1 3LE, United Kingdom

Abstract

A novel strong electron-acceptor unit, 9,10-difluorodithieno[3,2-*a*:2',3'-*c*]phenazine (DTPz), is synthesized and applied in the design of two donor-acceptor type emitters displaying long-lived delayed emission. Using either 9,9-dimethyl-9,10-dihydroacridine (DMAC) or triisopropyl-substituted benzo[1,2-*b*:4,5-*b'*]dithiophene (BDT-TIPS) as the donor component, push-pull type chromophores exhibiting charge-transfer emission are obtained and found to afford either thermally activated delayed fluorescence (TADF) for DMAC or room temperature phosphorescence (RTP) for BDT-TIPS.

Introduction

Since the advent of phosphorescent organic light-emitting diodes (PhOLEDs), this technology has found its way into everyday applications such as smartphone and television screens and solid-state lighting.[1-3] While strong spin-orbit coupling (SOC) associated with heavy-metal complexes allows efficient harvesting of electrically generated triplet states for emission (and corresponding high device efficiencies), PhOLEDs rely on rare-earth metals to achieve this and can therefore not be considered a sustainable technology. The use of heavy metals also contributes significantly to the cost of manufacture, raises health concerns related to their disposal, and fundamentally limits their applicability for deep-blue OLEDs due to electrochemical instability of the metal-ligand bonds.[4]

In 2009, Adachi *et al.*[5] applied the known mechanism of E-type delayed fluorescence[6, 7] or thermally activated delayed fluorescence (TADF)[8] to organic electroluminescent devices for the first time. By harvesting otherwise non-emissive triplet states, TADF materials increased OLED efficiencies beyond the limits of normal fluorescence based devices and thus paved the way for a new generation of high-efficiency metal-free OLEDs.[9-11] Triplet harvesting in TADF materials is achieved by decreasing the overlap between the highest occupied and lowest unoccupied molecular orbitals (HOMO and LUMO, respectively) of the emissive material, thus reducing the energy difference between the singlet and triplet excited states (ΔE_{ST}). When ΔE_{ST} is small enough, spin-forbidden intersystem crossing (ISC) and reverse ISC (rISC) become more active and interconversion between the singlet and triplet states occurs.[12] Because of the minute presence of SOC in these systems, slow phosphorescence channels are usually not active at room temperature (they are outcompeted by rISC and singlet TADF emission) and fluorescence is the main relaxation pathway. Since ISC and rISC are forbidden transitions between orbitals of the same nature,[13] two triplets states of different orbital character close in energy are required to allow so-called vibronic mixing.[14-16] These mixed states are then allowed to undergo (r)ISC with the singlet state.

From a molecular design perspective, spatial separation of the HOMO and LUMO is most easily achieved by combining donor (electron-rich) and acceptor (electron-poor) moieties *via* a bridge that is electronically decoupled due to highly twisted bonding, spiro-linkage, or homoconjugation.[9, 12, 17, 18] In such systems, the HOMO can be found on the donor part, whereas the LUMO typically resides on the acceptor unit. This leads to accessible charge-transfer (CT) excited states, which together with locally excited triplet states (^{3}LE) of similar energy on the donor or acceptor provide the necessary conditions for adequate rISC rates to emerge. Improper energy level alignment can lead to other properties such as triplet-triplet annihilation (TTA) or room temperature phosphorescence (RTP).

The combinatorial nature of donor-acceptor (D-A) or donor-acceptor-donor (D-A-D) TADF materials implies that a nearly infinite number of combinations are possible. While high-performance TADF materials are now regularly reported,[19-33] further performance improvements are still desirable, especially for deep-blue[34] and red or near-infrared[29, 35] emission. Seeking inspiration from other fields of organic electronics such as organic photovoltaics,[36-39] we have used the 9,10-difluorodithieno[3,2-*a*:2',3'-*c*]phenazine (DTPz) scaffold as a novel strong TADF acceptor unit, to which 9,9-dimethyl-9,10-dihydroacridine (DMAC) was coupled through a Buchwald-Hartwig type reaction. Additionally, a recently reported triisopropylsilyl-functionalized benzo[1,2-*b*:4,5-*b'*]dithiophene (BDT) unit was used as an alternative donor in a Suzuki cross-coupling reaction with DTPz.[40] Quantum-chemical calculations showed a small overlap between the HOMO and LUMO for both D-A combinations. Experimentally, TADF or RTP behavior is observed dependent on the donor unit and the resultant alignment of singlet and triplet excited state energy levels.

Results and discussion

DTPz, **DTPz-BDT-TIPS**[41] and DMAC[42] were prepared using previously reported methods. Coupling was done via Buchwald-Hartwig (DMAC) or Suzuki (BDT-TIPS) cross-coupling reactions (Scheme 1). Full synthetic details can be found in the supporting information.

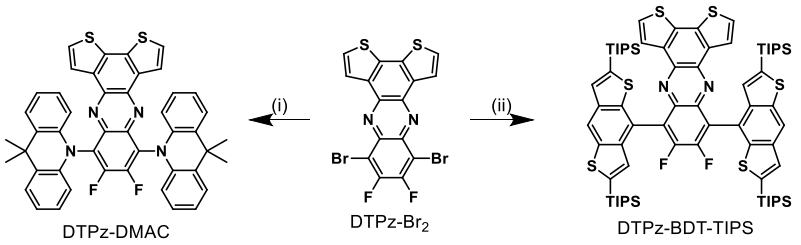

Scheme 1: Synthesis pathways toward **DTPz-DMAC** and **DTPz-BDT-TIPS** (TIPS = triisopropylsilyl): (i) 9,9-dimethyl-9,10-dihydroacridine, $Pd(OAc)_2$, XPhos, NaO*t*Bu, toluene, 110 °C, 24 h; (ii) BDT-TIPS-pinacol, $Pd(PPh_3)_4$, K_2CO_3, DMF/H_2O 4/1, 130 °C, 24 h.

The geometries of the DTPz acceptor and the two D-A-D chromophores were optimized using density functional theory (DFT) calculations with M06/6-311G(d).[43] Time dependent DFT (TDDFT) calculations were performed to calculate the singlet and triplet energies using a modified LC-BLYP (ω = 0.17 bohr^{-1})[41, 44, 45] XC functional with 6-311G(d) as the basis set under the Tamm-Dancoff approximation[46, 47]. The modified LC-BLYP (ω = 0.17 bohr^{-1}) was optimized for TADF emitters in previous work.[41, 44] TDDFT calculations were performed using the polarizable continuum model (PCM) (cyclohexane) to simulate a non-polar environment. Gas-phase TDDFT calculations were performed using the same method (Table S1), revealing a minor influence (0.01 - 0.04 eV) from the PCM on the excitation energies. All calculations were performed using the Gaussian16 package.[48] The CT character of the involved states for the D-A-D compounds was calculated according to the work of Le Bahers *et al.*[49] Here, the difference between the ground and excited state densities is taken to represent individual transitions, visualizing the regions of increased/decreased electron density upon promotion from the ground state to an excited state. These density differences allow us to identify the donor and acceptor parts of the molecule in a (CT) transition and enable estimation of the degree of charge-transfer character through d_{CT}. However, the differentiation between CT and LE states can only be performed by comparing the values within a given set of similar molecules as d_{CT} and $\Delta\mu$ will adopt different values as the molecular structure changes and are impacted by properties such as symmetry.

The optimized geometries (Figure 1) show large dihedral angles, around 85° for **DTPz-DMAC**, as often seen for DMAC-based compounds,[50] and around 59° for **DTPz-BDT-TIPS**. The smaller dihedral angles for the BDT-TIPS donor were also observed in previous work and are due to the decrease in donor steric hindrance for the five-membered fused rings.[40] The triisopropyl groups, although bulky, are not expected to hinder the vibrational modes of the BDT group as they are facing away from the acceptor unit. Furthermore, the acceptor acts as a spacer between the two BDT groups, and from the optimized geometries (Figure 1) it is apparent that the TIPS groups on two adjacent BDT units do not influence each other. The HOMO and LUMO orbitals are well separated (Figure 1), suggesting strong CT character, which is further confirmed by looking at the nature of the first singlet vertical excitation energies and the CT distances (d_{CT}) (Table 1). The increase in dipole moment ($\Delta\mu$) between the ground and excited state densities further supports this interpretation. For **DTPz-BDT-TIPS**, the first triplet excited state shows localized character as indicated by the much smaller d_{CT} and $\Delta\mu$ values with respect to those of the first singlet excited state. This is also visualized by considering the difference between the ground and excited state electron densities (Figure S1), where the densities are clearly localized on the DTPz unit. The HOMO-1 and HOMO-2 spatial distributions are given in Figure S2 as they play a role in some of the other transitions under consideration here.

Table 1: Nature of the various transitions (H = HOMO, L = LUMO), charge-transfer distance (d_{CT}) and change in dipole moment ($\Delta\mu$, excited – ground state dipole) accompanying the $S_0 \rightarrow S_x$ and $S_0 \rightarrow T_x$ transitions in cyclohexane.

	S_1			S_2			T_1			T_2		
Compound	Nature	d_{CT} (Å)	$\Delta\mu$ (D)	Nature	d_{CT} (Å)	$\Delta\mu$ (D)	Nature	d_{CT} (Å)	$\Delta\mu$ (D)	Nature	d_{CT} (Å)	$\Delta\mu$ (D)
DTPz-DMAC	H→L	1.53	8.37	H-1→L	1.54	8.58	H→L	1.51	8.00	H-1→L	1.54	8.56
DTPz-BDT-TIPS	H→L	2.06	10.82	H-1→L	2.01	10.67	H-2→L	0.29	0.64	H→L	1.46	5.14

Table 2: TDDFT results for the vertical first and second singlet excitation energies and corresponding oscillator strengths, and the vertical first and second triplet excitation energies.

Compound	S_1 (eV)	f_{S_1}	S_2 (eV)	f_{S_2}	T_1 (eV)	T_2 (eV)	$\Delta E_{T_2-T_1}$ (eV)	$\Delta E_{S_1-T_1}$ (eV)
DTPz-DMAC	2.20	0.00	2.23	0.00	2.17	2.22	0.05	0.03
DTPz-BDT-TIPS	2.73	0.05	2.83	0.02	2.30	2.55	0.25	0.43
DTPz	3.11	0.10	3.23	0.00	2.37	2.77	0.40	0.74

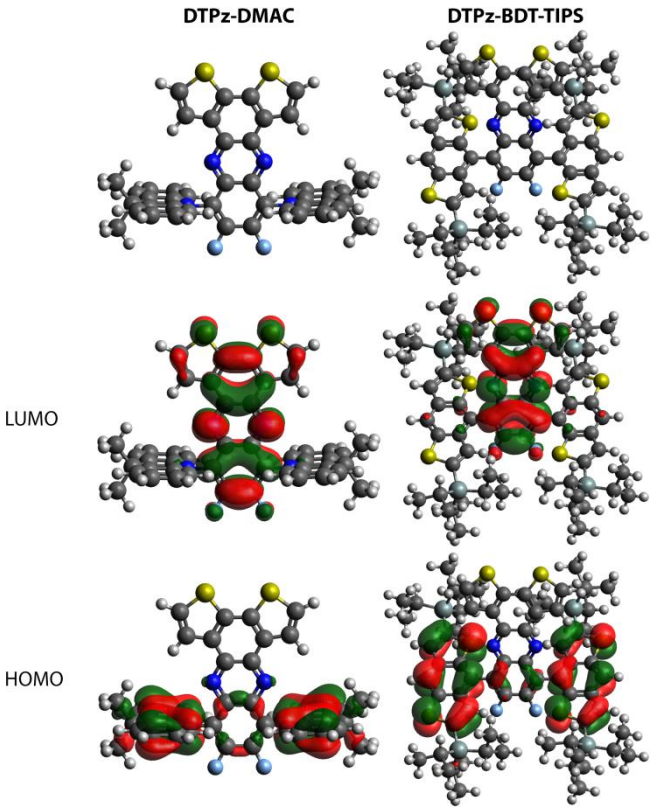

Figure 1: HOMO and LUMO spatial distributions for **DTPz-DMAC** and **DTPz-BDT-TIPS** as obtained with LC-BLYP(ω=0.17)/6-311G(d). Isocontour values of 0.02 (a.u.) were used for all orbitals.

The TDDFT calculations predict singlet excitation energies of 2.20 eV (564 nm) for **DTPz-DMAC** and 2.73 eV (454 nm) for **DTPz-BDT-TIPS** (Table 2). **DTPz-DMAC** was found to have a theoretical ΔE_{ST} of 0.03 eV, whereas that of **DTPz-BDT-TIPS** is 0.43 eV. The acceptor DTPz was also included in the calculations, affording singlet and triplet excitation energies of 3.11 and 2.37 eV, respectively. From the analysis of the CT character of the excited states, we observed localization of the first excited triplet state of **DTPz-BDT-TIPS** on the acceptor (Figure S1). Therefore, we expected a similar excitation energy for this state as for the non-functionalised acceptor unit, which is confirmed by the calculations (Table 2). For **DTPz-DMAC**, the first triplet state is of CT character with electron density being transferred from the DMAC to the DTPz parts of the compound (Figure S1). UV-VIS absorption spectra were simulated (Figure S3) and are dominated by the LE bands which are higher in energy than the aforementioned CT states. Their profiles are in agreement with the experimental spectra (Figure 2).

From the steady-state emission spectra in zeonex film, a broad and unstructured emission band is visible for both compounds (Figure 2). A distinct shift is observed between **DTPz-DMAC** and **DTPz-BDT-TIPS**, the onset of the former being red-shifted by nearly 77 nm (0.33 eV), indicating stronger CT character for the DMAC donor. Solvatochromism was investigated by measuring the steady-state emission in solvents of varying polarity, which is indicative of CT state emission for both materials (Figure S4). No significant solvent effect was observed for the UV-VIS absorption spectra, indicating the LE character of these absorption bands.

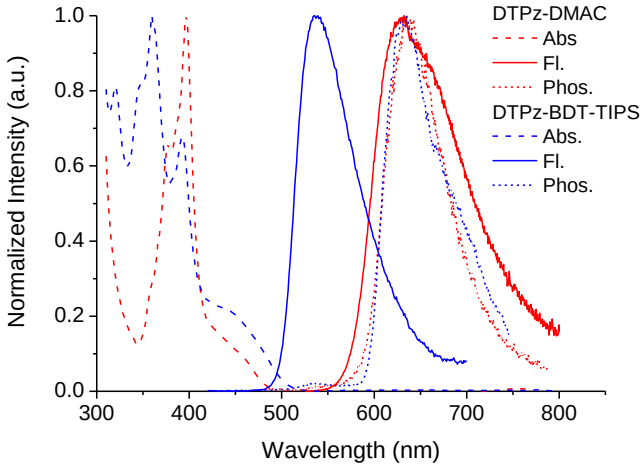

Figure 2: Steady-state absorption (dashed lines) and emission (full lines) spectra at room temperature and time-resolved emission at a 44.7 ms delay time at 80 K (dotted lines) in zeonex film for **DTPz-DMAC** (red) and **DTPz-BDT-TIPS** (blue).

Table 3: Photophysical properties and kinetics for **DTPz-DMAC** and **DTPz-BDT-TIPS** in zeonex film and photoluminescence quantum yields in toluene solution.

Compound	E_S (eV)[a]	E_T (eV)[b]	ΔE_{ST} (eV)[c]	τ_{Fp} (ns)[d]	τ_{Fd} (µs)[e]	k_{ISC} (s^{-1})[f]	k_{rISC} (s^{-1})[f]	$\Phi_{f,inert}$[h]
DTPz-DMAC	2.16	2.11	0.05	8.4	422.6	$7.8x10^7$	$2.5x10^5$	0.03 (0.01)
DTPz-BDT-TIPS	2.49	2.09	0.40	4.3	$2.6x10^4$	—[g]	—[g]	0.01 (0.01)

[a] Taken from the onset of the prompt fluorescence. [b] Taken from the onset of the phosphorescence at ms timescales at 80 K. [c] Calculated as $E_S - E_T$. [d] Lifetime of prompt fluorescence (F_p). [e] Lifetime of delayed fluorescence (F_d). [f] k_{ISC} and k_{rISC} were determined using kinetic fitting of the prompt and delayed fluorescence according to literature.[51] [g] Cannot be determined due to the lack of TADF emission. [h] Fluorescence quantum yield under inert atmosphere (and normal atmosphere in brackets) in toluene solution determined vs quinine (Φ_f = 0.58, λ_{exc} = 347 nm) in 0.1 M H_2SO_4.

In Figure 3a,b the contour maps of the normalized time-resolved emission spectra of **DTPz-DMAC** in zeonex at room temperature and at 80 K are shown. After a fast decaying prompt emission, the intensity falls below the sensitivity limit of the camera. At several microseconds and with longer integration times, the signal reappears at exactly the same wavelength as the prompt emission at room temperature and persists until around 12 milliseconds. In Figure 3c, the decay of the total emission intensity is plotted. At 80 K, the emission drops below the sensitivity of the iCCD after approximately 50 nanoseconds and it is not until several hundreds of microseconds that a new red-shifted emission band appears (attributed to phosphorescence and plotted in Figure 2). Figure S5 shows individual spectra taken at various delay times, showing a clear difference in onset between the room temperature and 80 K delayed emission. The lack of microsecond delayed emission at 80 K is consistent with a TADF mechanism being disrupted by the lack of available thermal energy at these temperatures, and phosphorescence emission instead dominating at longer times. Calculating ΔE_{ST} from the onsets of the fluorescence and phosphorescence emission (Table 3), a rather small gap of 0.05 eV is found, which is in good agreement with the quantum-chemical calculations. The long lifetime of the delayed emission at room temperature (422.6 µs) likely arises from slow rISC, which is confirmed by kinetic fitting of the room temperature decay. The low rate of rISC in this material, despite its low ΔE_{ST}, demonstrates that energy gaps alone are not a proper indicator of strong TADF performance.[52]

DTPz-BDT-TIPS shows a very different behavior in zeonex films. Only short-lived green prompt CT emission followed by a long-lived orange delayed emission is observed (Figure 3d,e,f and Figure S6). The long micro- to millisecond emission can be attributed to phosphorescence rather than delayed fluorescence, as the spectra at room temperature and 80 K show the same structured peak shape and onset (Figure 4 and Figure S6). Additionally, a small contribution likely arising from triplet-triplet annihilation (TTA) can be seen at around 535 nm in the room temperature delayed spectra (Figure S6). TTA is suspected as the emission mechanism as the onset of this delayed emission band is similar to that of the prompt emission. The lack of TADF emission is not surprising given the much larger theoretical ΔE_{ST} for this material (0.43 eV). The experimental ΔE_{ST} calculated from the onset of the prompt fluorescence at room temperature and the phosphorescence at 80 K is 0.40 eV (Table 3) and is in good agreement with the calculations. Similar observations were also made for TXO2-BDT-TIPS in previous work, where the lowest triplet excited state was found to be localized on BDT-TIPS and the donor unit itself showed RTP.[40] However, in this work, the difference between the ground and excited state electron densities reveals that the first excited triplet state is localized on the DTPz acceptor rather than on the BDT donor for **DTPz-BDT-TIPS** (Figure S1). Therefore, the phosphorescence likely originates from the acceptor core and not from the BDT-TIPS donor in this case. To help further understand the emitting states in these materials, the DTPz acceptor itself (without bromine atoms) was also subjected to time-resolved emission spectroscopy and was found to exhibit phosphorescence at room temperature (Figure 4). Given the presence of sulfur atoms in the DTPz core, it is plausible that the resulting increased SOC is sufficient to allow radiative relaxation through a T_1->S_0 pathway on the acceptor. Comparing the phosphorescence spectra of BDT-TIPS, DTPz

and **DTPz-BDT-TIPS** (Figure 4) further supports the interpretation that the RTP of the D-A material comes from excitons localized on the acceptor rather than on the donor. It is, however, possible that an excited state localized on the BDT-TIPS unit still acts as the main intersystem crossing pathway (as it did for TXO2-BDT-TIPS in our previous study) in **DTPz-BDT-TIPS**, followed by internal conversion to the localized DTPz state. This is likely as the second triplet state shows some delocalization on the BDT-TIPS unit and has an energy that is below the theoretical vertical excitation energy of the first singlet state.

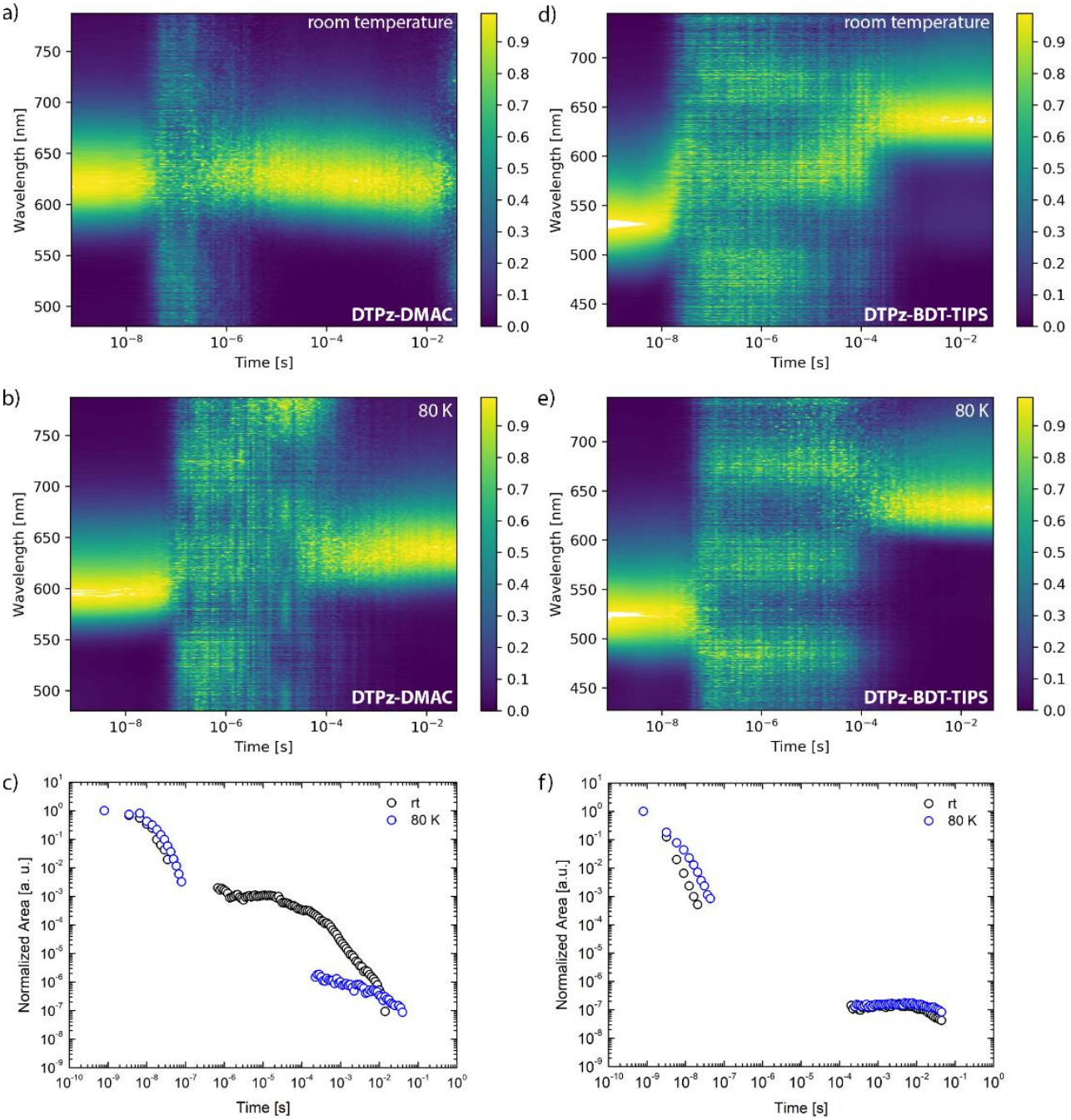

Figure 3: Normalized time-resolved emission spectra for **DTPz-DMAC** (left) and **DTPz-BDT-TIPS** (right) in zeonex at room temperature (a,d) and at 80 K (b,e). Decays of the total emission for **DTPz-DMAC** (c) and **DTPz-BDT-TIPS** (f) at room temperature (rt) and at 80 K in zeonex.

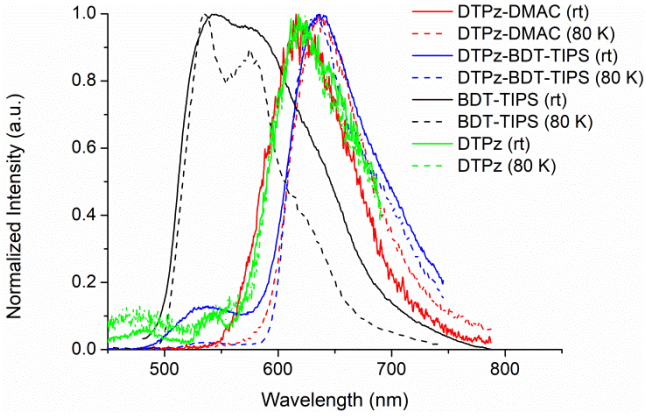

Figure 4: Overlap of the emission spectra at 44.7 ms for **DTPz-DMAC**, **DTPz-BDT-TIPS**, DTPz and BDT-TIPS at room temperature and at 80 K in zeonex.

The full decays as a function of normalized total emission in zeonex versus time are shown in Figure 3c and 3f. For **DTPz-DMAC**, a clear difference is seen between the decays at room temperature and 80 K. The relatively high intensity, very long-lived emission is indicative of a thermally activated process with a slow rate of rISC. **DTPz-BDT-TIPS** shows virtually no emission in the microsecond domain in zeonex films. At longer times, a small emission contribution is observed, illustrative of RTP behavior (as outlined above). This emission is insensitive to cryogenic temperatures, again indicating that it does not arise from TADF.

In addition to the thin film measurements, photoluminescence quantum yields were determined in toluene solution in normal and inert atmosphere to gauge the luminescent capabilities of the novel emitters (Table 3). Despite the low quantum yields, **DTPz-DMAC** does show an increase in emission when going from normal to inert atmosphere, suggesting the presence of a triplet upconversion mechanism under inert atmosphere (as oxygen is known to quench triplet states). For **DTPz-BDT-TIPS**, this is not observed, in agreement with the proposed RTP mechanism.

Finally, the dependence of the delayed fluorescence intensity with respect to the excitation laser power was determined for both compounds in zeonex film. For **DTPz-DMAC**, the measurement was done at a 5 µs delay time and 750 µs integration time and shows a linear power law dependence with a slope of 1 (Figure S7). This result indicates that we are not observing TTA in this time domain. **DTPz-BDT-TIPS** did not show any early microsecond emission. Therefore, we probed the late microseconds to milliseconds domain with a 630 µs delay time and 10 ms integration time to determine whether the main delayed emission could be attributed to RTP instead of TTA. However, from the time-resolved spectral measurements at room temperature and at 80 K we could already conclude that this emission band is most likely due to phosphorescence. The laser power measurement further solidified these observations (Figure S7).

Conclusions

We have synthesized two new D-A-D compounds based on the 9,10-difluorodithieno[3,2-*a*:2',3'-*c*]phenazine (DTPz) acceptor. This acceptor was coupled to the strong TADF donor 9,9-dimethyl-9,10-dihydroacridine (DMAC) and a weaker benzo[1,2-*b*:4,5-*b'*]dithiophene (BDT-TIPS) donor. Photophysical analysis showed that both compounds exhibit long-lived delayed emission in a zeonex film. **DTPz-DMAC** was found to exhibit TADF properties. Despite a small singlet-triplet energy gap (0.05 eV), the rate of reverse intersystem crossing is rather small, leading to long-lived delayed fluorescence. **DTPz-BDT-TIPS** was found to show RTP from the acceptor unit at room temperature in a nonpolar zeonex matrix. Although the materials do not display ideal TADF properties for OLED applications, their long-lived and red-shifted emission indicates that they can be used for other applications such as imaging, sensing or security inks.[53-56] Combined with other appropriate donor groups and suitable hosts, DTPz may be valuable in the continuing pursuit of efficient deep-red TADF materials for OLEDs.

Conflicts of interest

The authors declare no competing financial interest.

Acknowledgements

This work is supported by the University of Namur and Hasselt University (PhD BILA scholarship T. Cardeynaels). The authors also thank the Research Foundation – Flanders (FWO Vlaanderen) for financial support (projects G087718N, G0D1521N, I006320N, GOH3816NAUHL, and SB PhD scholarship S. Paredis). The calculations were performed on the computers of the « Consortium des équipements de Calcul Intensif *(CÉCI)* » (http://www.ceci-hpc.be), including those of the « UNamur Technological Platform of High-Performance Computing (PTCI) » (http://www.ptci.unamur.be), for which we gratefully acknowledge the financial support from the FNRS-FRFC, the Walloon Region, and the University of Namur (Conventions No. 2.5020.11, GEQ U.G006.15, U.G018.19, 1610468, and RW/GEQ2016). A. Danos and A.P. Monkman are supported by EU Horizon 2020 Grant Agreement No. 732103 (HyperOLED).

Supporting information

Detailed information about the synthesis procedures, calculated gas-phase excitation energies, ground/excited state electron density differences, HOMO and LUMO spatial distributions and energies, simulated UV-VIS absorption spectra, steady-state absorption and fluorescence spectra in different solvents, time-resolved photoluminescence data, laser power experiments, ^{1}H and ^{13}C NMR spectra, and coordinates of the optimized geometries can be found in the supporting information.

References

[1] Bizzarri C, Hundemer F, Busch J, Bräse S. Triplet emitters versus TADF emitters in OLEDs: A comparative study. Polyhedron. 2018;140:51-66.

[2] Brütting W, Frischeisen J, Schmidt TD, Scholz BJ, Mayr C. Device efficiency of organic light-emitting diodes: Progress by improved light outcoupling. physica status solidi (a). 2013;210(1):44-65.

[3] Hyocheol J, Hwangyu S, Jaehyun L, Beomjin K, Young-Il P, Kyoung Soo Y, et al. Recent progress in the use of fluorescent and phosphorescent organic compounds for organic light-emitting diode lighting. Journal of Photonics for Energy. 2015;5(1):1-23.

[4] Seifert R, Rabelo de Moraes I, Scholz S, Gather MC, Lüssem B, Leo K. Chemical degradation mechanisms of highly efficient blue phosphorescent emitters used for organic light emitting diodes. Organic Electronics. 2013;14(1):115-23.

[5] Endo A, Ogasawara M, Takahashi A, Yokoyama D, Kato Y, Adachi C. Thermally activated delayed fluorescence from Sn(4+)-porphyrin complexes and their application to organic light emitting diodes--a novel mechanism for electroluminescence. Adv Mater. 2009;21(47):4802-6.

[6] Lewis GN, Lipkin D, Magel TT. Reversible Photochemical Processes in Rigid Media. A Study of the Phosphorescent State. Journal of the American Chemical Society. 1941;63(11):3005-18.

[7] Parker CA, Hatchard CG. Triplet-singlet emission in fluid solutions. Phosphorescence of eosin. Transactions of the Faraday Society. 1961;57(0):1894-904.

[8] Nishikawa Y, Hiraki K, Onoue Y, Nishikawa K, Yoshitake Y, Shigematsu T. DELAYED FLUOROMETRIC ANALYSIS OF CHLOROPHYLL C AND PHEOPHYTIN C. Bunseki kagaku. 1983;32(4):E115-E22.

[9] Liu Y, Li C, Ren Z, Yan S, Bryce MR. All-organic thermally activated delayed fluorescence materials for organic light-emitting diodes. Nature Reviews Materials. 2018;3(4):18020.

[10] Bui T-T, Goubard F, Ibrahim-Ouali M, Gigmes D, Dumur F. Recent advances on organic blue thermally activated delayed fluorescence (TADF) emitters for organic light-emitting diodes (OLEDs). Beilstein Journal of Organic Chemistry. 2018;14:282-308.

[11] Wong MY, Zysman-Colman E. Purely Organic Thermally Activated Delayed Fluorescence Materials for Organic Light-Emitting Diodes. Advanced Materials. 2017;29(22):1605444.

[12] Penfold TJ, Dias FB, Monkman AP. The theory of thermally activated delayed fluorescence for organic light emitting diodes. Chem Commun (Camb). 2018;54(32):3926-35.

[13] Baba M. Intersystem crossing in the 1npi* and 1pipi* states. J Phys Chem A. 2011;115(34):9514-9.

[14] Gibson J, Monkman AP, Penfold TJ. The Importance of Vibronic Coupling for Efficient Reverse Intersystem Crossing in Thermally Activated Delayed Fluorescence Molecules. Chemphyschem. 2016;17(19):2956-61.

[15] Penfold TJ, Gindensperger E, Daniel C, Marian CM. Spin-Vibronic Mechanism for Intersystem Crossing. Chem Rev. 2018;118(15):6975-7025.

[16] Etherington MK, Gibson J, Higginbotham HF, Penfold TJ, Monkman AP. Revealing the spin-vibronic coupling mechanism of thermally activated delayed fluorescence. Nat Commun. 2016;7:13680.

[17] Adachi C. Third-generation organic electroluminescence materials. Japanese Journal of Applied Physics. 2014;53(6):060101.

[18] Kawasumi K, Wu T, Zhu T, Chae HS, Van Voorhis T, Baldo MA, et al. Thermally Activated Delayed Fluorescence Materials Based on Homoconjugation Effect of Donor-Acceptor Triptycenes. J Am Chem Soc. 2015;137(37):11908-11.

[19] Stachelek P, Ward JS, Dos Santos PL, Danos A, Colella M, Haase N, et al. Molecular Design Strategies for Color Tuning of Blue TADF Emitters. ACS Appl Mater Interfaces. 2019;11(30):27125-33.

[20] Miwa T, Kubo S, Shizu K, Komino T, Adachi C, Kaji H. Blue organic light-emitting diodes realizing external quantum efficiency over 25% using thermally activated delayed fluorescence emitters. Scientific Reports. 2017;7(1):284.

[21] Kim JU, Park IS, Chan C-Y, Tanaka M, Tsuchiya Y, Nakanotani H, et al. Nanosecond-time-scale delayed fluorescence molecule for deep-blue OLEDs with small efficiency rolloff. Nature Communications. 2020;11(1):1765.

[22] Sun D, Suresh SM, Hall D, Zhang M, Si C, Cordes DB, et al. The design of an extended multiple resonance TADF emitter based on a polycyclic amine/carbonyl system. Materials Chemistry Frontiers. 2020.

[23] Zhu X-D, Peng C-C, Kong F-C, Yang S-Y, Li H-C, Kumar S, et al. Acceptor modulation for improving a spiro-type thermally activated delayed fluorescence emitter. Journal of Materials Chemistry C. 2020.

[24] Zheng X, Huang R, Zhong C, Xie G, Ning W, Huang M, et al. Achieving 21% External Quantum Efficiency for Nondoped Solution-Processed Sky-Blue Thermally Activated Delayed Fluorescence OLEDs by Means of Multi-(Donor/Acceptor) Emitter with Through-Space/-Bond Charge Transfer. Advanced Science. 2020;7(7):1902087.

[25] Huang W, Einzinger M, Maurano A, Zhu T, Tiepelt J, Yu C, et al. Large Increase in External Quantum Efficiency by Dihedral Angle Tuning in a Sky-Blue Thermally Activated Delayed Fluorescence Emitter. Advanced Optical Materials. 2019;7(20):1900476.

[26] Lee KH, Jeon SO, Chung YS, Numata M, Lee H, Lee EK, et al. An excited state managing molecular design platform of blue thermally activated delayed fluorescence emitters by π-linker engineering. Journal of Materials Chemistry C. 2020;8(5):1736-45.
[27] Yu JG, Han SH, Lee HL, Hong WP, Lee JY. A novel molecular design employing a backbone freezing linker for improved efficiency, sharpened emission and long lifetime in thermally activated delayed fluorescence emitters. Journal of Materials Chemistry C. 2019;7(10):2919-26.
[28] Gong X, Li P, Huang Y-H, Wang C-Y, Lu C-H, Lee W-K, et al. A Red Thermally Activated Delayed Fluorescence Emitter Simultaneously Having High Photoluminescence Quantum Efficiency and Preferentially Horizontal Emitting Dipole Orientation. Advanced Functional Materials. 2020;30(16):1908839.
[29] Kim D-H, D'Aléo A, Chen X-K, Sandanayaka ADS, Yao D, Zhao L, et al. High-efficiency electroluminescence and amplified spontaneous emission from a thermally activated delayed fluorescent near-infrared emitter. Nature Photonics. 2018;12(2):98-104.
[30] Chen J-X, Tao W-W, Chen W-C, Xiao Y-F, Wang K, Cao C, et al. Red/Near-Infrared Thermally Activated Delayed Fluorescence OLEDs with Near 100 % Internal Quantum Efficiency. Angewandte Chemie International Edition. 2019;58(41):14660-5.
[31] Kim JH, Lee KH, Lee JY. Design of Thermally Activated Delayed Fluorescent Assistant Dopants to Suppress the Nonradiative Component in Red Fluorescent Organic Light-Emitting Diodes. Chemistry – A European Journal. 2019;25(38):9060-70.
[32] Zhang Y-L, Ran Q, Wang Q, Liu Y, Hänisch C, Reineke S, et al. High-Efficiency Red Organic Light-Emitting Diodes with External Quantum Efficiency Close to 30% Based on a Novel Thermally Activated Delayed Fluorescence Emitter. Advanced Materials. 2019;31(42):1902368.
[33] Kothavale S, Chung WJ, Lee JY. Rational Molecular Design of Highly Efficient Yellow-Red Thermally Activated Delayed Fluorescent Emitters: A Combined Effect of Auxiliary Fluorine and Rigidified Acceptor Unit. ACS Applied Materials & Interfaces. 2020;12(16):18730-8.
[34] Huang R, Kukhta NA, Ward JS, Danos A, Batsanov AS, Bryce MR, et al. Balancing charge-transfer strength and triplet states for deep-blue thermally activated delayed fluorescence with an unconventional electron rich dibenzothiophene acceptor. Journal of Materials Chemistry C. 2019;7(42):13224-34.
[35] Congrave DG, Drummond BH, Conaghan PJ, Francis H, Jones STE, Grey CP, et al. A Simple Molecular Design Strategy for Delayed Fluorescence toward 1000 nm. J Am Chem Soc. 2019;141(46):18390-4.
[36] Po R, Bianchi G, Carbonera C, Pellegrino A. "All That Glisters Is Not Gold": An Analysis of the Synthetic Complexity of Efficient Polymer Donors for Polymer Solar Cells. Macromolecules. 2015;48(3):453-61.
[37] Efrem A, Wang K, Amaniampong PN, Yang C, Gupta S, Bohra H, et al. Direct arylation polymerization towards narrow bandgap conjugated microporous polymers with hierarchical porosity. Polymer Chemistry. 2016;7(30):4862-6.
[38] Fan J, Zhang Y, Lang C, Qiu M, Song J, Yang R, et al. Side chain effect on poly(beznodithiophene-co-dithienobenzoquinoxaline) and their applications for polymer solar cells. Polymer. 2016;82:228-37.
[39] Zhang Y, Zou J, Yip H-L, Chen K-S, Davies JA, Sun Y, et al. Synthesis, Characterization, Charge Transport, and Photovoltaic Properties of Dithienobenzoquinoxaline- and Dithienobenzopyridopyrazine-Based Conjugated Polymers. Macromolecules. 2011;44(12):4752-8.
[40] Cardeynaels T, Paredis S, Danos A, Vanderzande D, Monkman AP, Champagne B, et al. Benzo[1,2-b:4,5-b']dithiophene as a weak donor component for push-pull materials displaying thermally activated delayed fluorescence or room temperature phosphorescence. Dyes and Pigments. 2021;186:109022.
[41] Cardeynaels T, Paredis S, Deckers J, Brebels S, Vanderzande D, Maes W, et al. Finding the optimal exchange-correlation functional to describe the excited state properties of push-pull organic dyes designed for thermally activated delayed fluorescence. Phys Chem Chem Phys. 2020;22(28):16387-99.
[42] Deckers J, Cardeynaels T, Penxten H, Ethirajan A, Ameloot M, Kruk M, et al. Near-Infrared BODIPY-Acridine Dyads Acting as Heavy-Atom-Free Dual-Functioning Photosensitizers. Chemistry. 2020;26(66):15212-25.
[43] Zhao Y, Truhlar DG. The M06 suite of density functionals for main group thermochemistry, thermochemical kinetics, noncovalent interactions, excited states, and transition elements: two new functionals and systematic testing of four M06-class functionals and 12 other functionals. Theoretical Chemistry Accounts. 2008;120(1):215-41.
[44] Penfold TJ. On Predicting the Excited-State Properties of Thermally Activated Delayed Fluorescence Emitters. The Journal of Physical Chemistry C. 2015;119(24):13535-44.
[45] Iikura H, Tsuneda T, Yanai T, Hirao K. A long-range correction scheme for generalized-gradient-approximation exchange functionals. The Journal of Chemical Physics. 2001;115(8):3540-4.
[46] Hirata S, Head-Gordon M. Time-dependent density functional theory within the Tamm–Dancoff approximation. Chemical Physics Letters. 1999;314(3):291-9.
[47] Bauernschmitt R, Ahlrichs R. Treatment of electronic excitations within the adiabatic approximation of time dependent density functional theory. Chemical Physics Letters. 1996;256(4):454-64.
[48] M. J. Frisch GWT, H. B. Schlegel, G. E. Scuseria, M. A. Robb, J. R. Cheeseman, G. Scalmani, V. Barone, G. A. Petersson, H. Nakatsuji, X. Li, M. Caricato, A. V. Marenich, J. Bloino, B. G. Janesko, R. Gomperts, B. Mennucci, H. P. Hratchian, J. V. Ortiz, A. F. Izmaylov, J. L. Sonnenberg, D. Williams-Young, F. Ding, F. Lipparini, F. Egidi, J. Goings, B. Peng, A. Petrone, T. Henderson, D. Ranasinghe, V. G. Zakrzewski, J. Gao, N. Rega, G. Zheng, W. Liang, M. Hada, M. Ehara, K. Toyota, R. Fukuda, J. Hasegawa, M. Ishida, T. Nakajima, Y. Honda, O. Kitao, H. Nakai, T. Vreven, K. Throssell, J. A. Montgomery, Jr., J. E. Peralta, F. Ogliaro, M. J. Bearpark, J. J. Heyd, E. N. Brothers, K. N. Kudin, V. N. Staroverov, T. A. Keith, R. Kobayashi, J. Normand, K.

Raghavachari, A. P. Rendell, J. C. Burant, S. S. Iyengar, J. Tomasi, M. Cossi, J. M. Millam, M. Klene, C. Adamo, R. Cammi, J. W. Ochterski, R. L. Martin, K. Morokuma, O. Farkas, J. B. Foresman, and D. J. Fox. Gaussian 16, Revision A.03. Wallingford CT: Gaussian, Inc.; 2016.
[49] Le Bahers T, Adamo C, Ciofini I. A Qualitative Index of Spatial Extent in Charge-Transfer Excitations. J Chem Theory Comput. 2011;7(8):2498-506.
[50] Kukhta NA, Higginbotham HF, Matulaitis T, Danos A, Bismillah AN, Haase N, et al. Revealing resonance effects and intramolecular dipole interactions in the positional isomers of benzonitrile-core thermally activated delayed fluorescence materials. Journal of Materials Chemistry C. 2019;7(30):9184-94.
[51] Haase N, Danos A, Pflumm C, Morherr A, Stachelek P, Mekic A, et al. Kinetic Modeling of Transient Photoluminescence from Thermally Activated Delayed Fluorescence. The Journal of Physical Chemistry C. 2018;122(51):29173-9.
[52] Ward JS, Nobuyasu RS, Batsanov AS, Data P, Monkman AP, Dias FB, et al. The interplay of thermally activated delayed fluorescence (TADF) and room temperature organic phosphorescence in sterically-constrained donor–acceptor charge-transfer molecules. Chemical Communications. 2016;52(12):2612-5.
[53] Xiong X, Song F, Wang J, Zhang Y, Xue Y, Sun L, et al. Thermally activated delayed fluorescence of fluorescein derivative for time-resolved and confocal fluorescence imaging. J Am Chem Soc. 2014;136(27):9590-7.
[54] Crucho CIC, Avó J, Nobuyasu R, N. Pinto S, Fernandes F, Lima JC, et al. Silica nanoparticles with thermally activated delayed fluorescence for live cell imaging. Materials Science and Engineering: C. 2020;109:110528.
[55] Wu Y, Jiao L, Song F, Chen M, Liu D, Yang W, et al. Achieving long-lived thermally activated delayed fluorescence in the atmospheric aqueous environment by nano-encapsulation. Chemical Communications. 2019;55(96):14522-5.
[56] Lei Y, Dai W, Guan J, Guo S, Ren F, Zhou Y, et al. Wide-Range Color-Tunable Ultralong Organic Phosphorescence Materials for Printable and Writable Security Inks. Angewandte Chemie International Edition. 2020;n/a(n/a).